Influence of Wettability on Electrical Parameters Based on Numerical Simulation Results of Drainage and Imbibition in Digital Rock

Tatyana Khachkova[1(✉)] and Vadim Lisitsa[2]

[1] Institute of Petroleum Geology and Geophysics SB RAS, Koptug ave. 3, Novosibirsk 630090, Russia
KhachkovaTS@ipgg.sbras.ru

[2] Institute of Mathematics SB RAS, Koptug ave. 4, Novosibirsk 630090, Russia

Abstract. The present study investigates the influence of wettability on the hysteresis of electrical parameters through numerical simulation of drainage and imbibition processes. Using a three-dimensional digital sandstone sample and numerical algorithms for simulating two-phase filtration and electric current flow, a series of numerical experiments are conducted over a full range of contact angles. The dependence of the resistivity index on the water saturation is then established for each value of angle, and the parameters of Archie's law – namely, the saturation exponent and the saturation distribution factor – are estimated. The principle objective is to derive functional relationships between these parameters and the contact angle. The resulting dependencies are constructed as piecewise linear functions, exhibiting different trends for drainage and imbibition. Validation at intermediate contact angles revealed that the relative errors of the estimates remain below 3%.

Keywords: Wettability · Electrical parameters · Resistivity index · Saturation exponent · Water saturation · Digital models · Numerical simulation · Drainage · Imbibition · CT-images

1 Introduction

Numerical simulation of physical processes has become an indispensable tool across various scientific disciplines, including exploration geophysics. It enables the computation of physical fields necessary for estimating petrophysical properties of porous media. Traditionally, such estimates have relied on laboratory core analysis; however, this approach is labor-intensive, time-consuming, and often results in irreversible damage or complete failure of rock samples.

Recent advances in X-ray microtomography have enabled the construction of three-dimensional digital rock models that accurately replicate the microstructure of natural samples. These digital twins serve as a realistic basis for numerical

© The Author(s), under exclusive license to Springer Nature Switzerland AG 2027
O. Gervasi et al. (Eds.): ICCSA 2026 Workshops, LNCS 16761, pp. 98–110, 2027.
https://doi.org/10.1007/978-3-032-30527-5_7

simulations. To date, a wide range of algorithms have been developed for estimating key petrophysical parameters, including porosity, absolute permeability [2,6,12,16], relative permeability [1,3,10], elastic moduli [2,7,18,20], electrical resistivity [2,8,22], pore space geometry and topology [5], and etc. These tools enable researchers to investigate the inter-parameter relationships, the influence of various factors on petrophysical estimates, and to predict of reservoir behavior under changing conditions.

The present study employs digital rock physics to investigate the effect of wettability on the electrical parameters during two-phase flow. In hydrocarbon exploration, reserves are typically estimated from electrical logging data interpreted using Archie's empirical laws. Consequently, accurate determination of Archie's parameters – namely, the saturation exponent and the saturation distribution factor – is of critical importance for reservoir development planning. The saturation exponent is known to depend on several factors: microstructure (heterogeneity, pore connectivity, pore size distribution), wettability, the presence of cement, and pore water salinity. In laboratory experiments, isolating the individual effects of microstructure and wettability is extremely challenging. Moreover, systematically studying the influence of the entire spectrum of contact angles – beyond the conventional classification of rocks as hydrophilic, hydrophobic, neutrally wet, or mixed-wet – is practically infeasible. However, such a detailed investigation is essential, as wettability governs fluid distribution and flow patterns, particularly under conditions of enhanced oil recovery by imbibition.

It should also be noted that prolonged field development leads to reservoir hydrophobization. Consequently, accounting for wettability alterations – particularly their spatial heterogeneity – is essential for reservoir monitoring and the timely adjustment of production strategies. This, in turn, necessitates the development of novel numerical methodologies that enable rapid and reliable determination of the saturation exponent and saturation distribution factor as functions of varying wettability.

The present paper proposes a new approach for refining these parameters, based on numerical modeling of steady-state two-phase flow and subsequent simulation of electrical current flow. A series of numerical experiments is conducted to construct the dependence of the resistivity index on water saturation for a range of contact angles. This enables a systematic investigation of the effect of wettability on the hysteresis observed during displacement of the wetting phase (drainage) and the non-wetting phase (imbibition). The primary objective of this study is to derive new functional relationships that enhance the reliability of saturation exponent estimates. The obtained dependencies will contribute to more accurate assessments of recoverable hydrocarbon reserves, improve the construction of hydrodynamic reservoir models, and support the selection of optimal reservoir stimulation techniques for enhanced hydrocarbon recovery.

2 Methodology

The methodology for establishing the dependence of electrical parameters on rock wettability is based on numerical simulations of primary drainage and imbibition processes within a digital rock sample. The results of these simulations are utilized to generate models of partially saturated rock and to calculate the corresponding electrical parameters, namely the resistivity index and the saturation exponent. This section provides a brief description of the basic algorithms employed in this workflow.

2.1 Algorithm for Numerical Simulation of Two-Phase Flows

To simulate primary drainage and subsequent imbibition, a three-dimensional numerical algorithm for pore-scale simulation of two-phase flows is employed [9,10]. The algorithm is based on the phase field method, in which concentration functions are used to identify the phases, and a thin transition region (smoothed over several grid cells) defines the boundary between them.

To simulate the fluid flow in the pore space, the Stokes equation is considered, with the nonlinear term neglected due to the low flow velocity:

$$\begin{aligned} &\frac{\partial \rho(\psi)\boldsymbol{u}}{\partial t} = -\nabla p + 2\nabla \cdot (\nu\epsilon(\boldsymbol{u})) + \boldsymbol{G}(\psi), \\ &\nabla \cdot (\boldsymbol{u}) = 0. \end{aligned} \tag{1}$$

In these equations, $\psi \in [0,1]$ is the phase-determining concentration function, $\rho(\psi)$ is the fluid density, $\nu(\psi)$ is the fluid viscosity, $\boldsymbol{u}$ is the vector of velocity, p is the pressure, $2\epsilon(u) = \nabla \boldsymbol{u} + \nabla \boldsymbol{u}^T$ is doubled strain tensor, $\boldsymbol{G}(\psi)$ are external forces. It was assumed that gravitational forces could be neglected; so that external forces were caused only by surface tension at the phase boundary.

To simulate the phase field, the Cahn-Hilliard equation is considered:

$$\begin{aligned} &\frac{\partial \psi}{\partial t} + \boldsymbol{u} \cdot \nabla \psi = \nabla \cdot (M(\psi)\nabla \mu), \\ &\mu = F'(\psi) - \varepsilon^2 \Delta \psi, \end{aligned} \tag{2}$$

where μ denotes the variable for determining the chemical potential, M is the mobility, ε is the width of the diffuse boundary between phases. For the potential $F(\psi)$ it is employed the expression $F'(\psi) = 2\psi(\psi-1)(2\psi-1)$, and for the external forces related to the interfacial surface tension: $\boldsymbol{G}(\psi) = -\frac{6\sqrt{2}}{\varepsilon}\psi\nabla\mu$.

Since the present study is aimed at investigating the influence of wettability on electrical parameters, the algorithm for simulating two-phase flows was modified by incorporating a new boundary condition at the liquid-solid interface (rock matrix). This condition accounts for the phase contact angle, thereby enabling a more accurate representation of phase dynamics at low wetting angles [19,21]:

$$\nabla \psi \cdot \boldsymbol{n} = -\frac{\sqrt{2}\pi \cos((\psi-0.5)\pi)}{12\varepsilon} \cos(\theta), \tag{3}$$

where θ is the contact angle for the first phase.

The finite-difference approximation was described in detail in earlier works [9,10]. It was also noted that the proposed finite-difference scheme provides first-order approximation in both time and space, employing a simplest upwind scheme for the spatial approximation of the phase transfer. For the purposes of the present study, the order of spatial approximation was improved by implementing a more accurate third-order WENO scheme [14,17].

The implementation of the described algorithm was designed for use on graphics processing units (GPUs) and was carried out in CUDA. Recently, the algorithm has been further improved with respect to solving the Poisson equation; this enhancement is described in more detail in the following subsection.

2.2 Algorithm for Numerical Simulation of Electric Current and Evaluation of Electrical Resistivity

The fundamentals of the algorithm for the numerical evaluation of electrical resistivity in digital rock samples were presented in [8]. This algorithm was developed specifically for application to strongly heterogeneous models, such as digital rock samples. To numerically estimate the resistivity of core samples, the electric potential distribution is first calculated under an applied voltage difference imposed on opposite faces of the sample. Then, the conductivity is estimated as the ratio of the resulting electric current to the applied voltage difference. The most computationally demanding and complex component of this algorithm is the calculation of the electric potential, which requires solving the Poisson equation in a domain characterized by a highly heterogeneous medium. Such a medium is defined as one in which the characteristic size of heterogeneities spans only a few grid cells, namely, where the correlation length of the model ranges from five to ten grid points [4]. Moreover, the amplitude of these inhomogeneities may vary by several orders of magnitude.

The approach proposed in [8] is based on a Krylov-type iterative solver, which employs the inverse of the discrete Laplace operator for a homogeneous medium as a preconditioner. To invert the Laplace operator, spectral decomposition along the directions normal to the current flow is applied, followed by the Thomas algorithm to solve a series of one-dimensional problems. A development of this approach with respect to the numerical solution of the Poisson equation was presented in [13]. In new improved version, the Conjugate Gradient method was employed in place of BiCGStab, spectral decomposition of the discretized operator was used instead of its continuous one, and cuBLAS functionality was also utilized. As a result, the proposed approach significantly increases the size of digital samples that can be processed on a single GPU while simultaneously reducing computation time.

The next improvement to this algorithm concerns the construction of a preconditioner for the numerical solution of the Poisson equation [15]. Employing the inverted Laplace operator for a layered medium (instead of homogeneous one) as a preconditioner reduces the number of iterations required by the Conjugate Gradient method by 10–40%. Moreover, the efficiency of this approach improves with increasing contrast in the coefficients of the digital model. Given

that in models partially saturated with water and oil, the electrical conductivities of water, oil and the rock matrix differ by several orders of magnitude, the convergence rate was substantially enhanced through the use of this method.

It should also be noted that this approach was adopted to improve the algorithm for simulation of two-phase flows, as it likewise requires the efficient solution of Poisson equations.

2.3 Numerical Simulation of Primary Drainage and Imbibition

Primary drainage is a process in which a non-wetting phase displaces a wetting one. Conversely, during imbibition, the wetting phase displaces the non-wetting one. In an oil-water system considered for numerical simulation, water represents the wetting phase, while oil represents the non-wetting one.

Thus, during drainage, oil displaces water. The numerical simulation of primary drainage begins with a model fully saturated with water, and only oil is injected into the digital sample. This simulation replicates processes occurring in nature, when a water-saturated reservoir gradually becomes charged with oil migrating from a source rock. As a result of drainage, oil displaces the mobile water, leaving the irreducible water saturation S_{irr}.

Starting from this state, imbibition is then simulated, during which water begins to displace oil. In this part of study, a laboratory experiment on steady-state two-phase filtration is numerically reproduced, with water being gradually introduced into the mixture. Under this approach, imbibition is represented not as a single numerical (or laboratory) experiment, but as a series of experiments. At each stage, the proportion of water in the injected mixture is increased; for instance, in a series of ten experiments, the water fractions are 0.1, 0.2, ... 1. At the final stage, only water is injected into the sample. As a result of imbibition, water displaces all mobile oil, reaching the residual oil saturation S_{res}.

All experiments are conducted until steady-state flow is achieved. For the numerical simulations performed using the two-phase flow algorithm, steady-state conditions are assumed to be reached after five pore volumes of fluid have been pumped through the sample.

2.4 Numerical Evaluation of the Resistivity Index and the Saturation Exponent

During the numerical experiments, phase distributions across the sample volume are recorded. For the drainage process, 15 snapshots are taken, including the final state, as the evolution of the process itself is of interest. For the imbibition, only the final state following each injection mode is recorded, resulting in 10 snapshots in this case.

From the obtained phase distributions, the current water saturations S_w, as well as the irreducible water saturation S_{irr} and the residual oil saturation S_{res}, are determined. These distributions are subsequently used to construct partially saturated water-oil models for the purpose of calculating electrical parameters.

Using the algorithm for numerical simulation of electric current, the electrical resistivity is then computed for all partially saturated models. In addition, the same calculation is performed for a fully water-saturated model, i.e., a model in which all pores are numerically filled with water. Based on these results, the resistivity index is estimated according to the following formula:

$$RI = \frac{\rho_t}{\rho_0}, \tag{4}$$

where ρ_t is the electrical resistivity at a given water saturation S_w, and ρ_0 is the resistivity of the fully water-saturated rock.

Thus, two sets of values, $S_w - RI(S_w)$, are obtained: one for drainage and one for imbibition. To estimate the saturation exponent, the classical form of Archie's law for the resistivity index is employed:

$$RI(S_w) = S_w^{-n}, \tag{5}$$

where n is the saturation exponent, along with the generalized form of Archie's law:

$$RI(S_w) = \alpha S_w^{-n}, \tag{6}$$

where α is the saturation distribution factor. The methodology for estimating the saturation exponent has been described in detail in [11]. It is based on constructing a linear regression on a logarithmic scale using the obtained datasets and solving two optimization problems corresponding to the classical and generalized formulations of Archie's law.

Given that the objective of this study is to investigate the influence of wettability on electrical parameters, the described methodology is applied to estimate the parameters of Archie's law for both drainage and imbibition across different wetting angles.

3 Numerical Experiments

For all numerical experiments conducted in this study, a digital model of Bentheimer sandstone was employed. The model dimensions are $200 \times 750 \times 750$ voxels, with a microtomographic images resolution of 2 μm per voxel. As previously noted, water (wetting phase) and oil (non-wetting one) were considered as the two phases in the flow simulation. The following physical parameters were assigned to water and oil, respectively: densities of 1000 kg/m^3 and 880 kg/m^3, dynamic viscosities of $3.8 \cdot 10^{-4}$ $Pa \cdot s$ and $4.027 \cdot 10^{-3}$ $Pa \cdot s$, and an interfacial tension of $2.571 \cdot 10^{-2}$ N/m. The contact angles for the water phase were selected from the set $[20, 30, 40, 50, 60, 70, 80, 90]$ degrees. For each contact angle, a separate series of simulations was performed. Two-phase flow was simulated in the X direction, with a constant flow rate of $1.225 \cdot 10^{-8}$ m^3/s specified at the inlet face.

Subsequently, for all obtained partially saturated models, the electrical resistivity was computed using formula 4. In the numerical algorithm for simulating

electric current, the following electrical conductivity values were assigned to water, oil and the rock matrix, respectively: 1 S, $1 \cdot 10^{-3}$ S and $1 \cdot 10^{-5}$ S.

As a result of the numerical experiments, sets of $S_w - RI(S_w)$ values for both drainage and imbibition were obtained for each contact angle within the set $[20, 30, 40, 50, 60, 70, 80, 90]$.

The following section presents the processing and analysis of the results from these numerical experiments.

3.1 Construction of Dependencies: Resistivity Index Versus Water Saturation and Saturation Exponent Versus Contact Angle

First, the dependencies of the resistivity index on water saturation were established for all specified contact angles. That is, linear regressions were constructed on a logarithmic scale by solving two optimization problems corresponding to the classical (Eq. 5) and generalized forms of Archie's law (Eq. 6).

The results for contact angles of 20 and 60 are presented in the Figs. 1 and 2, respectively. The blue lines correspond to the drainage simulation results, while the violet lines represent the imbibition results. Solid lines denote the generalized Archie's law, whereas dashed lines indicate the classical formulation of Archie's law.

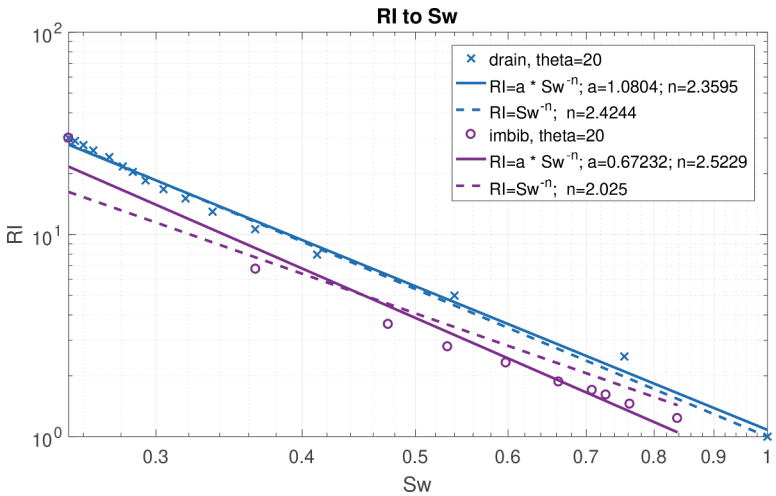

Fig. 1. Dependence of the resistivity index on water saturation for Bentheimer sandstone during drainage and imbibition simulation at a water contact angle of $\theta = 20°$ (logarithmic scales).

Thus, for each contact angle, the following parameters were estimated: the saturation exponent n_{cl} corresponding to the classical form of Archie's law (Eq. 5), as well as the saturation exponent n and the saturation distribution

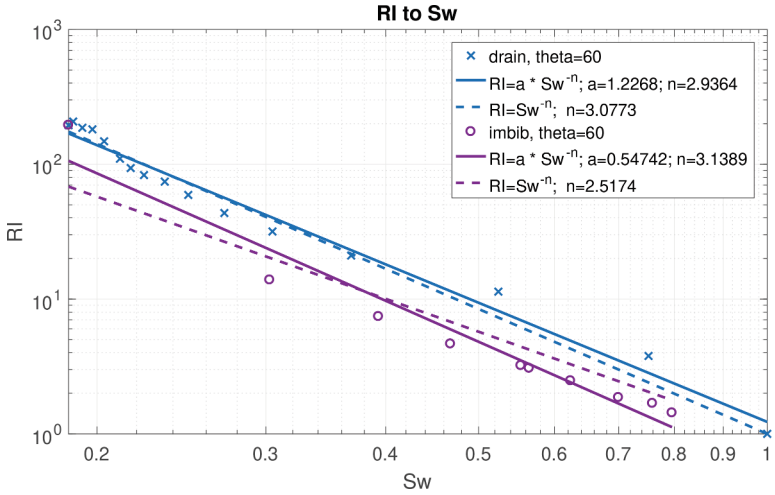

Fig. 2. Dependence of the resistivity index on water saturation for Bentheimer sandstone during drainage and imbibition simulation at a water contact angle of $\theta = 60°$ (logarithmic scales).

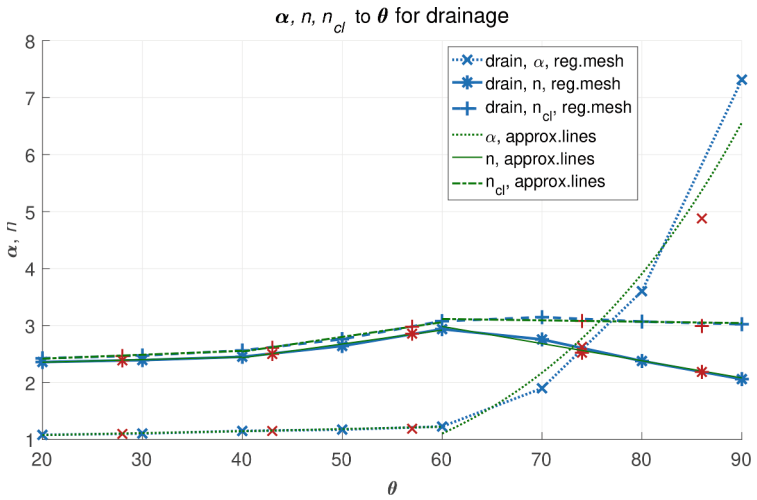

Fig. 3. Dependence of Archie's parameters on contact angle for Bentheimer sandstone based on drainage simulation results.

factor α corresponding to the generalized form (Eq. 6). The obtained values are presented in Figs. 3 and 4, with blue and violet markers, respectively.

In Figs. 3 and 4, it can be observed that the dependencies of Archie's parameters on the contact angle are piecewise linear, with the solo exception being the parameter α for drainage within the range of 60 to 90°. Therefore, this particular dependence was approximated by constructing a linear regression on a

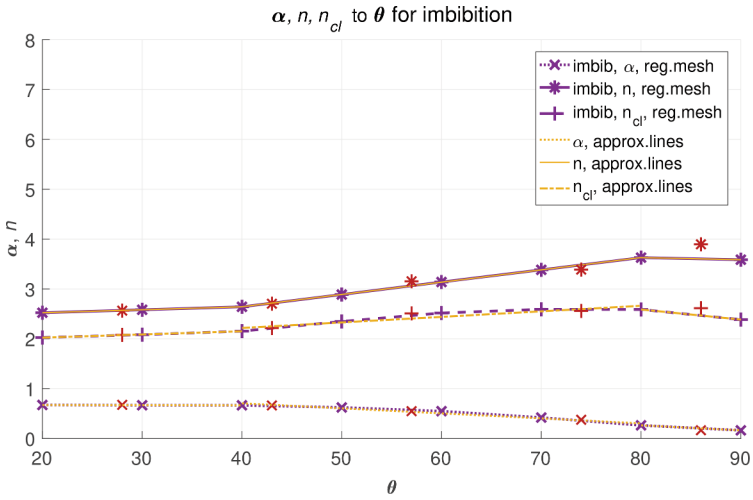

Fig. 4. Dependence of Archie's parameters on contact angle for Bentheimer sandstone based on imbibition simulation results.

logarithmic scale, whereas all other dependencies were approximated using linear functions. The resulting approximation lines are shown in green (for drainage) in Fig. 3, and in yellow (for imbibition) in Fig. 4. The corresponding approximation formulas are presented in Table 1.

To validate the obtained dependencies, a series of additional numerical experiments was conducted, following the same methodology as before but employing contact angles between the previously selected grid points, specifically, $\theta = 28$, 43, 57, 74 and 86°. As in the primary simulations, the electrical parameters were calculated and the values of Archie's parameters were estimated then. These results are shown in Figs. 3 and 4 using red markers. Subsequently, the relative errors in the estimation of these parameters using the derived approximation formulas were computed. The obtained values for all specified angles and parameters are presented in Table 1. The angle values used for validation are indicated in red.

Analysis of the 30 relative error values reveals that the majority are below 3%: 14 values are less than 1%, and 10 values lie between 2% and 3%. Only 5 values fall within the 5–10% range. Notably, these elevated errors correspond to all parameters at $\theta = 86$ (in the case of imbibition), and solely to the parameter α at $\theta = 74$ and $\theta = 86$ (for drainage).

In the imbibition case, the red markers corresponding to $\theta = 86$ in Fig. 4 extend the straight lines fitted for the 40–80 range. This observation suggests that the linear dependencies may be applicable up to 90°, despite possible changes in fluid behavior near $\theta = 90$. A correction was implemented, and the revised formulas for the angle of $\theta = 86$ produced relative errors of 2–3% (see the lower rows of Table 1).

Table 1. Dependence of Archie's parameters on contact angle for Bentheimer sandstone: approximation formulas and validation relative errors.

θ	α	Rel.err.	n	Rel.err.	n_{cl}	Rel.err.
Drainage						
20–40	$0.0034 \cdot \theta + 1$		$0.0046 \cdot \theta + 2.26$		$0.0069 \cdot \theta + 2.28$	
28		0.0066		0.002		0.0038
40–60	$0.0039 \cdot \theta + 0.99$		$0.024 \cdot \theta + 1.46$		$0.026 \cdot \theta + 1.51$	
43		0.0061		0.0024		0.0041
57		0.0185		0.0036		0.00058
60–90	$e^{4.4 \cdot ln(\theta) - 17.91}$		$-0.03 \cdot \theta + 4.79$		$-0.0024 \cdot \theta + 3.26$	
74		0.0563		0.0158		0.00067
86		0.101		0.0074		0.0206
Correction						
60–70	$0.0671 \cdot \theta - 2.8$					
70–89	$0.186 \cdot \theta - 11.143$					
74		0.0069				
80		0.04				
Imbibition						
20–40	$0.0003 \cdot \theta + 0.68$		$0.0059 \cdot \theta + 2.4$		$0.0064 \cdot \theta + 1.895$	
28		0.0086		0.0022		0.0022
40–80	$-0.01 \cdot \theta + 1.108$		$0.025 \cdot \theta + 1.655$		$0.011 \cdot \theta + 1.77$	
43		0.0189		0.0047		0.0157
57		0.0249		0.0289		0.0412
74		0.0336		0.0277		0.0144
80–90	$-0.01 \cdot \theta + 1.07$		$-0.0042 \cdot \theta + 3.96$		$-0.02 \cdot \theta + 4.2$	
86		0.053		0.0750		0.0565
Correction						
80–89	$-0.01 \cdot \theta + 1.108$		$0.025 \cdot \theta + 1.655$		$0.011 \cdot \theta + 1.77$	
86		0.034		0.0233		0.0326

For drainage, a logarithmic scale was initially employed for the approximation. However, a linear approximation may also be considered, as the point for α at $\theta = 86$ (marked in red in Fig. 3) approximately extends the line trend for 70–80 range. A correction was introduced by constructing piecewise linear functions for the intervals of 60–70 and 70–86°. The values at $\theta = 74$ and $\theta = 80$ were used as validation points (the correction is highlighted in green in Table 1). Such approximation resulted in relative errors of 0.6% and 4%, respectively.

The resulting piecewise linear approximations are summarized in Table 2.

Table 2. Summary of approximations for Archie's parameters as functions of contact angle for Bentheimer sandstone.

θ	α	n	n_{cl}
Drainage			
20–40	$0.0034 \cdot \theta + 1$	$0.0046 \cdot \theta + 2.26$	$0.0069 \cdot \theta + 2.28$
40–60	$0.0039 \cdot \theta + 0.99$	$0.024 \cdot \theta + 1.46$	$0.026 \cdot \theta + 1.51$
60–70	$0.0671 \cdot \theta - 2.8$	$-0.03 \cdot \theta + 4.79$	$-0.0024 \cdot \theta + 3.26$
70–89	$0.186 \cdot \theta - 11.143$		
Imbibition			
20–40	$0.0003 \cdot \theta + 0.68$	$0.0059 \cdot \theta + 2.4$	$0.0064 \cdot \theta + 1.895$
40–89	$-0.01 \cdot \theta + 1.108$	$0.025 \cdot \theta + 1.655$	$0.011 \cdot \theta + 1.77$

4 Conclusions

The present study investigates the influence of wettability on the hysteresis of electrical parameters, specifically the resistivity index and the saturation exponent. Accurate estimation of these parameters is crucial, as they are employed both in the assessment of hydrocarbon reserves at the field and in reservoir development planning.

A digital model of Bentheimer sandstone (a high-permeability rock sample) is utilized in conjunction with two numerical algorithms: one for simulating two-phase flow and another for modeling electric current flow and estimating the corresponding electrical parameters. Initially, drainage and imbibition processes are numerically simulated, with the contact angle varying between 20 and 90°. The obtained numerical results are subsequently employed to construct digital models of partially water- and oil-saturated samples, for which electric current flow is simulated and electrical parameters are evaluated.

For each obtained model, the current water saturations, as well as the irreducible water saturations and the residual oil saturations are calculated, together with the corresponding values of the resistivity index. Based on these data, the dependencies of the resistivity index on the water saturation are established across the entire range of contact angles. Consequently, for each contact angle, the saturation exponent corresponding to the classical formulation of Archie's law is derived, as well as the saturation exponent and the saturation distribution factor for its generalized form.

The principal objective of this work is to establish the dependence of Archie's law parameters on the contact angle. These dependencies are constructed as piecewise linear functions for specific intervals of angles, with different trends observed for drainage and imbibition process.

To validate the derived dependencies, numerical experiments are conducted for intermediate contact angle values, with the calculation of the Archie's parameters and the associated relative errors. Based on an analysis of the obtained

errors, several formulas are corrected, thereby reducing the errors to an acceptable level of 3%.

In summary, this study demonstrates that Archie's law parameters – namely, the saturation exponent and the saturation distribution factor – are significantly dependent on the wettability of the rock. Moreover, hysteresis is observed in both parameters, as well as in the resistivity index, during drainage and imbibition process. The established functional dependencies enable the rapid and reliable determination of the key electrical parameters based on varying wettability, which is essential for reservoir monitoring and for timely adjustment of technological solutions.

Acknowledgments. T. Khachkova performed numerical simulations under the support of Russian Science Foundation grant no. 25-21-00352.

Disclosure of Interests. The authors have no competing interests to declare that are relevant to the content of this article.

References

1. Alpak, F.O., Riviere, B., Frank, F.: A phase-field method for the direct simulation of two-phase flows in pore-scale media using a non-equilibrium wetting boundary condition. Comput. Geosci. **20**(5), 881–908 (2016)
2. Andra, H., et al.: Digital rock physics benchmarks - Part II: computing effective properties. Comput. Geosci. **50**, 33–43 (2013)
3. Apourvari, S.N., Arns, C.H.: Image-based relative permeability upscaling from the pore scale. Adv. Water Resour. (2015)
4. Bazaikin, Y., et al.: Effect of CT image size and resolution on the accuracy of rock property estimates. J. Geophys. Res. Solid Earth **122**(5), 3635–3647 (2017)
5. Bazaikin, Y.V., Malkovich, E.G., Derevschikov, V.S., Lysikov, A.I., Okunev, A.G.: Evolution of sorptive and textural properties of CAO-based sorbents during repetitive sorption/regeneration cycles. Chem. Eng. Sci. **152**, 709–716 (2016)
6. Gerke, K.M., Karsanina, M.V., Katsman, R.: Calculation of tensorial flow properties on pore level: exploring the influence of boundary conditions on the permeability of three-dimensional stochastic reconstructions. Phys. Rev. E **100**(5), 053312 (2019)
7. Khachkova, T., Lisitsa, V., Reshetova, G.: Effect of interface roughness on the elastic properties of 3D layered media. Probab. Eng. Mech. **75**, 103571 (2024)
8. Khachkova, T., Lisitsa, V., Reshetova, G., Tcheverda, V.: GPU-based algorithm for evaluating the electrical resistivity of digital rocks. Comput. Math. Appl. **82**, 200–211 (2021)
9. Khachkova, T.S., Lisitsa, V.V.: Construction of relative permeability curves by numerical simulation of two-phase flow in 3D CT-models. Lecture Notes in Computer Science, vol. 14817, pp. 250–262 (2024). https://doi.org/10.1007/978-3-031-65238-7_17
10. Khachkova, T.S., Lisitsa, V.V., Gondul, E.A., Prokhorov, D.I., Kostin, V.I.: Two-phase flow simulation algorithm for numerical estimation of relative phase permeability curves of porous materials. Russ. J. Numer. Anal. Math. Model. **39**(4), 209–221 (2024). https://doi.org/10.1515/rnam-2024-0020

11. Khachkova, T.S., Lisitsa, V.V., Krutko, V.V., Avdonin, A.S.: Constructing dependence of electrical parameters on porosity and water saturation for digital models of high-permeability rock samples. Lecture Notes in Computer Science, vol. 15888, pp. 419–432 (2025). https://doi.org/10.1007/978-3-031-97596-7_28
12. Lisitsa, V., Khachkova, T., Sotnikov, O., Islamov, I., Ganiev, D.: Numerical evaluating the permeability of rocks based on correlation dependence on geometry. Lecture Notes in Computer Science, vol. 14106, pp. 91–102 (2023). https://doi.org/10.1007/978-3-031-37111-0_7
13. Lisitsa, V., Manaev, A., Solovyev, S.: Implementation of the spectral preconditioner to solve poisson equation. In: Gervasi, O., et al. (eds.) Computational Science and Its Applications – ICCSA 2025 Workshops, pp. 388–401. Springer (2025). https://doi.org/10.1007/978-3-031-97596-7_26
14. Luo, K., Zhuang, Z., Fan, J., Haugen, N.E.L.: A ghost-cell immersed boundary method for simulations of heat transfer in compressible flows under different boundary conditions. Int. J. Heat Mass Transf. **92**, 708–717 (2016)
15. Manaev, A.A., Lisitsa, V.V.: Spectral preconditioner for solving poisson equation. Comput. Methods Program. **26**(2), 111–128 (2025). https://doi.org/10.26089/NumMet.v26r208. (in Russian)
16. Mostaghimi, P., Blunt, M., Bijeljic, B.: Computations of absolute permeability on micro-CT images. Math. Geosci. **45**(1), 103–125 (2013)
17. Prokhorov, D., Lisitsa, V., Khachkova, T., Bazaikin, Y., Yang, Y.: Topology-based characterization of chemically-induced pore space changes using reduction of 3D digital images. J. Comput. Sci. **58**, 101550 (2022)
18. Saenger, E.H., et al.: Analysis of high-resolution X-ray computed tomography images of bentheim sandstone under elevated confining pressures. Geophys. Prospect. **64**(4), 848–859 (2016)
19. Shen, J., Yang, X., Yu, H.: Efficient energy stable numerical schemes for a phase field moving contact line model. J. Comput. Phys. **284**, 617–630 (2015)
20. Shulakova, V., et al.: Computational elastic up-scaling of sandstone on the basis of X-ray micro-tomographic images. Geophys. Prospect. **61**(2), 287–301 (2013)
21. Yu, H., Yang, X.: Numerical approximations for a phase-field moving contact line model with variable densities and viscosities. J. Comput. Phys. **334**, 665–686 (2017)
22. Zhan, X., Schwartz, L.M., Toksöz, M.N., Smith, W.C., Morgan, F.D.: Pore-scale modeling of electrical and fluid transport in berea sandstone. Geophysics **75**(5), F135–F142 (2010)